Non-Fickian Diffusion of Water in Nafion

ARTICLE *in* MACROMOLECULES · APRIL 2010

Impact Factor: 5.8 · DOI: 10.1021/ma100047z

5 AUTHORS, INCLUDING:

Daniel T. Hallinan
Florida State University
27 PUBLICATIONS **425** CITATIONS
SEE PROFILE

Maria Grazia De Angelis
University of Bologna
80 PUBLICATIONS **676** CITATIONS
SEE PROFILE

Marco Giacinti Baschetti
University of Bologna
69 PUBLICATIONS **642** CITATIONS
SEE PROFILE

Giulio C Sarti
University of Bologna
192 PUBLICATIONS **3,087** CITATIONS
SEE PROFILE

Macromolecules
ARTICLE

Macromolecules **2010**, *43*, 4667–4678 **4667**
DOI: 10.1021/ma100047z

Non-Fickian Diffusion of Water in Nafion

Daniel T. Hallinan, Jr.,[†] Maria Grazia De Angelis,[‡] Marco Giacinti Baschetti,[‡] Giulio C. Sarti,[‡] and Yossef A. Elabd*,[†]

[†]*Department of Chemical and Biological Engineering, Drexel University, 3141 Chestnut Street, Philadelphia, Pennsylvania 19104, and* [‡]*Dipartimento di Ingegneria Chimica, Mineraria e delle Tecnologie Ambientali Universitá di Bologna, Via Terracini 28, 40131 Bologna, Italy*

Received January 8, 2010; Revised Manuscript Received April 16, 2010

ABSTRACT: Understanding the dynamics of water in solid-state polymer electrolytes (e.g., Nafion) is important for a variety of applications ranging from membrane-based water purification to hydrogen fuel cells. In this study, the dynamics of water in Nafion was investigated at both low and high humidities with time-resolved Fourier transform infrared−attenuated total reflectance (FTIR−ATR) spectroscopy; a technique that provides a molecular fingerprint of both the diffusant and the polymer simultaneously in real time. At low humidities (0−22% RH), an extended initial time lag resulted in non-Fickian behavior, where dynamic infrared data provided evidence for a reaction between water and sulfonic acid. A diffusion−reaction model was developed and predicted this anomalous behavior, where the time lag was a function of water content. At high humidities (0−100% RH), a slow approach to steady state resulted in non-Fickian behavior, where dynamic infrared data provided evidence of water-induced relaxation in the polymer backbone. A diffusion−relaxation model was developed and regressed well to both the polymer relaxation and water diffusion data, where only one fitting parameter was used for each data set to determine both a relaxation time constant and diffusion coefficient. This approach differs significantly from previous work on non-Fickian behavior in glassy polymers, which, consisted of regressing gravimetric data to models with a minimum of six fitting parameters. Not only do the diffusion coefficients from these two models compare well with Fickian diffusion coefficients from experiments with small water concentration gradients, but also the results in this study provide physical insight into the transport mechanisms of water and relaxation phenomena in solid-state polymer electrolytes.

Introduction

Hydrogen polymer electrolyte membrane (PEM) fuel cells, where chemical energy is directly converted to electrical energy, provide a highly efficient alternative to standard internal combustion engines. High power densities, clean emissions (water), low-temperature operation, rapid start-up and shut-down times, and the ability to use fuels from renewable sources are several reasons why fuel cells have attracted attention for large market applications, such as transportation.[1] In the hydrogen fuel cell, a solid polymer (PEM) serves as the electrolyte, conducting protons from the anode to the cathode, but is also the key component that contributes to significant power losses at high temperatures (> 80 °C). Future fuel cells will use low-grade (inexpensive) hydrogen gas, which contain impurities (e.g., carbon monoxide) that poison precious metal anode catalysts (e.g., platinum) at low temperatures (< 120 °C) and reduce the overall fuel cell efficiency and power output.[2] In addition to mitigating catalyst poisoning, there are a number of other advantages to operating the PEM fuel cell at higher temperatures and lower humidities, such as increasing catalytic activity, reducing cathode flooding, and eliminating the need for external humidification equipment. Optimal fuel cell conditions for current PEMs (e.g., Nafion) are ∼80 °C and ∼100%RH. At higher temperatures, current PEMs dehydrate, reducing proton conductivity and overall cell performance.[3] Several investigators have proposed that future hydrogen PEM fuel cells will have to operate at conditions above 120 °C and below 40% relative humidity to truly be considered in the commercial marketplace.[1]

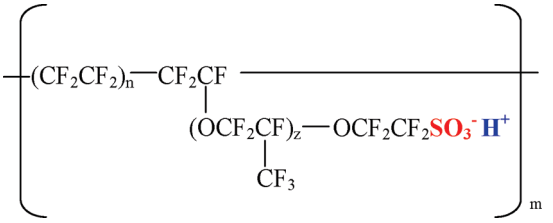

Figure 1. Chemical structure of Nafion.[65,66]

Currently, the most frequently used PEM in fuel cells is Nafion (Figure 1), a perfluorosulfonic acid polymer developed by DuPont in the 1960s.[4] Similar to many other sulfonic acid-based PEMs developed for fuel cells, Nafion exhibits sufficient proton conductivity (∼10^{-1} S/cm) when fully saturated with water, but significantly lower conductivity (by orders of magnitude) when equilibrated at lower water vapor activities.[5−7] Fuel cell performance is directly related to water balance (production, diffusion, and removal) in the system and, specifically to the water content in Nafion, not only in equilibrium conditions but also during the sorption and desorption processes as it applies to a dynamic system. Therefore, a fundamental understanding of water transport mechanisms in Nafion is desirable to aid in the development of PEMs that are highly conductive at high temperature, low humidity conditions.

Although similar water sorption isotherms in Nafion have been reproduced in many laboratories, reported diffusion coefficients

*To whom correspondence should be addressed. Telephone: 215.895.0986. Fax: 215.895.5837. E-mail: elabd@drexel.edu.

Published on Web 04/26/2010

of water in Nafion vary by 4 orders of magnitude.[5,6,8−20] In a recent study by Hallinan and Elabd,[21] sorption and desorption kinetics of water in Nafion were measured as a function of water vapor activity and flow rate using time-resolved Fourier transform infrared−attenuated total reflectance (FTIR−ATR) spectroscopy. One key result was that sorption kinetics was found to be a function of flow rate, where mass transfer resistance at the vapor/polymer interface was significant at low flow rates but insignificant at high flow rates. At high flow rates (no mass transfer resistance), accurate diffusion coefficients were calculated in this study and were weak functions of water vapor activity ($\sim 10^{-7}$ cm^2/s). Regressing low-flow rate data (with mass transfer resistance) to Fick's second law without accounting for boundary layer resistance resulted in diffusion coefficients an order of magnitude lower. This provides one reason for the discrepancy reported in literature, where numerous investigators have determined diffusivities from no-flow experiments without the appropriate boundary conditions in their model.

Additionally, in the study by Hallinan and Elabd,[21] both integral and differential experiments were performed, where integral experiments consisted of increasing vapor activity from a dry condition (0% RH) to one of several values (22, 43, 56, 80, or 100% RH) and differential experiments consisted of smaller activity changes increasing sequentially from 0 to 22 to 43 to 56 to 80 to 100% RH. In both types of experiments, Fickian diffusion behavior was observed at moderate humidity ranges (0−43, 0−56, 0−80, 22−43, 43−56, and 56−80% RH). Interestingly, two types of non-Fickian behavior were observed in this study. At low humidity (0−22% RH), the apparent non-Fickian behavior observed was due to an extended initial time lag that could not be predicted by Fickian sorption kinetics. It was proposed that this time lag might be the result of the reaction between water and sulfonic acid sites in Nafion when the initial water molecules sorb into dry Nafion.[21,22] The second and distinctively different type of non-Fickian behavior was observed for the high humidity integral experiments (0−100% RH), where water sorption had a slow approach to steady state. In comparison, the differential experiment at high humidity (80−100% RH) resulted in Fickian behavior. These results suggest that a rapid, large change in the concentration gradient from pseudoglassy, dry Nafion to 100% RH saturated induces stresses that are not present when a smaller concentration gradient was imposed from an already swollen state (80% RH saturated). This type of anomalous behavior (slow approach to steady state in the 0−100% RH experiment) has been observed by other investigators for the diffusion of organic vapors in glassy polymers and is indicative of diffusion and polymer relaxation occurring on similar time scales.[23]

In this study, the non-Fickian behavior observed at 0−22 and 0−100% RH was examined in more depth with more experiments, analysis, and modeling. Specifically, diffusion−reaction and diffusion−relaxation models were developed for the low and high vapor activity experiments, respectively. The dynamic FTIR−ATR data provides direct evidence for both the hydrolyzation reaction between water and sulfonic acid and also the water-induced relaxation in the polymer backbone. Diffusion−relaxation models have been developed in the past by other investigators,[23] but have usually consisted of regressing gravimetric data to models with a minimum of six fitting parameters. The results in this work are unique in that time-resolved FTIR−ATR spectroscopy provided both the polymer relaxation and water diffusion data and both were regressed to a newly developed diffusion−relaxation model, where only one fitting parameter was used for each data set. Additionally, the time-resolved FTIR−ATR data and models in this work provide new insights into the fundamental transport mechanisms of water in Nafion.

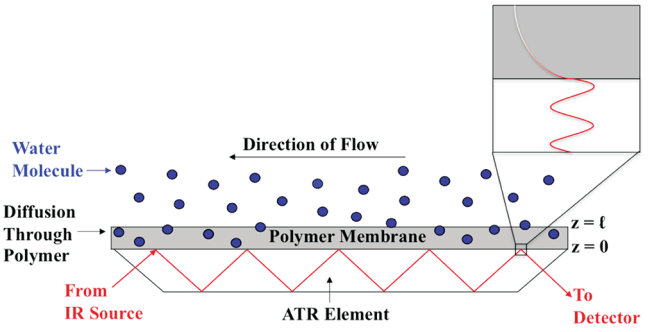

Figure 2. Schematic of ATR crystal and polymer. Evanescent wave highlighted in the magnified region.

Experimental Section

Materials. Nafion 117, hydrogen peroxide (30−32 wt %), sulfuric acid (99.999% purity, ACS reagent), and potassium acetate ($KC_2H_3O_2$ $1.5H_2O$; 99%) were purchased from Aldrich. Additionally, ultrapure reverse osmosis (RO) water (resistivity ~16 MΩ cm) and breathing quality compressed air (Airgas) was used. A glass moisture trap (Restek) packed with indicating Drierite and Molecular Sieve 5A was used to generate dry nitrogen.

Sample Preparation. Nafion 117 samples were cut into 6 × 1 cm pieces and subsequently purified similar to the procedure reported elsewhere.[21] This included successive steps of refluxing the samples in 3 wt % hydrogen peroxide, RO water, 1 M sulfuric acid, and RO water, where the samples were extensively rinsed with RO water after every reflux step and finally stored in separated RO water-filled vials.

Vapor Dilation. The dilation apparatus and setup are the same as described elsewhere.[24] A charge coupled device (CCD) camera was used to track the movement of two perpendicular sets of marks on a Nafion membrane, such that the change of length and width could be measured. The water activity was controlled by first evacuating all air from the system and then introducing pure water vapor from a pure water reservoir. The total pressure (due only to water vapor) was monitored with a pressure transducer, where the activity was the total pressure divided by the vapor pressure of water at 30 °C. The entire apparatus was maintained at 30 °C by a circulating water bath. Dilation measurements were used to calculate equilibrium Nafion density at each relative humidity of interest. Although dilation in the thickness direction could not be measured in vapor experiments, it was assumed to be the same as that in the width direction, supported by results from liquid dilation experiments, in which it was possible to measure dilation in all three directions. In liquid experiments, the width and thickness swelling were the same.[7]

Time-Resolved FTIR−ATR Spectroscopy. For diffusion experiments, time-resolved infrared spectra were collected using an FTIR spectrometer (Nicolet 6700 Series; Thermo Electron) equipped with a horizontal, temperature-controlled ATR cell (Specac, Inc.). A multiple reflection, trapezoidal (72 × 10 × 6 mm), zinc selenide (ZnSe) ATR crystal (Specac, Inc.) with 45° beveled faces (infrared angle of incidence, θ) was used. Infrared spectra were collected using a liquid nitrogen-cooled mercury−cadmium-telluride detector that collected 32 scans per spectrum at a resolution of 4 cm^{-1} (a spectrum was collected every 12.4 s). All spectra were corrected by a background subtraction of the ATR crystal spectrum. A schematic diagram of the ATR crystal and polymer is illustrated in Figure 2. At each reflection at the polymer/crystal interface, total internal reflection occurs, where an evanescent (exponentially decaying) electromagnetic wave exists within the polymer. The depth of penetration, d_p, or sampling depth into the polymer is the region in which the evanescent wave has decayed to 1/e the maximum intensity and is a function of the angle of incident

light, wavelength of light, and refractive indices of the crystal and polymer.

$$d_p = \left(\frac{\lambda}{2\pi n_{ZnSe} \sqrt{\sin^2(\theta) - (n_{Nafion}/n_{ZnSe})^2}} \right) \quad (1)$$

In this study, the refractive indices of the ATR element (ZnSe) and polymer are 2.4 (n_{ZnSe}) and 1.364 (n_{Nafion}), respectively, and the sampling depth is ~0.5−1 μm. The measured infrared absorbance is an integration of the electromagnetic field strength of this region in the polymer close to the polymer/crystal interface.[25]

Each diffusion experiment consisted of recording and saving a background spectrum of the ATR crystal for background subtraction. Then a prehydrated Nafion film was trimmed to the exact lateral dimensions of the ATR crystal (side-view of polymer/crystal interface is shown in Figure 2). The film was then physisorbed onto the crystal and secured in the flow-through ATR cell. A Kalrez gasket was used to ensure adequate adhesion between film and crystal and provide free space (550 uL) on the topside of the film for dry air to flow. Prior to each experiment, films were dried for 4 h at 30 °C with flowing dry air to ensure a dry steady state, adequate adhesion between film and crystal, and repeatable starting points for each diffusion experiment.

In this study, two different integral diffusion experiments were conducted: 0−22% RH and 0−100% RH. More specifically, to begin each integral experiment, at a carefully recorded time the dry air (0% RH) was removed and flowing air at a specific relative humidity (22 or 100% RH) was imposed on the vapor/polymer interface. Relative humidity was controlled by bubbling compressed purified air, at a controlled flow rate, through either a saturated aqueous salt solution of $KC_2H_3O_2$ (22% RH) or pure RO water (100% RH) through a tank (1000 mL, AceGlass), connector (30 cm long, AceGlass), and ATR cell. The temperature of the tank, connector and ATR cell were all carefully controlled at 30.0 ± 0.1 °C with a circulating water bath (NESLab RTE10). The flow rate was optimized to 150 mL/min to eliminate any mass transfer resistance at the interface without introducing any overpressure.[21] At this flow rate, the ATR cell was completely refreshed 58 times per data point (spectrum).

For this ATR system, unsteady-state Fickian diffusion of water in Nafion can be simply described by a one-dimensional continuity equation (Fick's second law):

$$\frac{\partial C}{\partial t} = D_{\text{eff}} \frac{\partial^2 C}{\partial z^2} \quad (2)$$

where C is concentration of the water, t is time, z is distance, and D_{eff} is the "effective" concentration-averaged diffusion coefficient. The initial and boundary conditions for the ATR configuration with a Nafion membrane of thickness, ℓ, exposed to an infinite reservoir of water with negligible mass transfer resistance (constant surface concentration) at the vapor/polymer interface and a no flux boundary condition at the polymer/ATR solid element interface are:

$$C = C_0 @ t = 0; \quad 0 < z < \ell \quad (3)$$

$$C = C_{eq} @ z = \ell; \quad t \geq 0 \quad (4)$$

$$\frac{dC}{dz} = 0 @ z = 0; t \geq 0 \quad (5)$$

The coordinates were chosen such that, $z = 0$ at the polymer/ATR element interface and z = ℓ for the vapor/polymer interface. For all diffusion experiments, C_0 equals the concentration of water in Nafion equilibrated at 0% RH and 30 °C. An analytical solution to eq 2 with these initial and boundary conditions is given:

$$\frac{C - C_0}{C_{eq} - C_0} = 1 - \frac{4}{\pi} \times \sum_{n=0}^{\infty} \frac{(-1)^n}{2n+1} \exp(-D_{eff} f^2 t) \cos(fz) \quad (6)$$

$$\text{where } f = \frac{(2n+1)\pi}{2\ell} \quad (7)$$

For weak IR absorption, concentration is related to absorbance through the differential Beer−Lambert law and incorporates the evanescent wave of the ATR infrared light:[25]

$$A(t) = \int_0^{\ell} \varepsilon \times C(t) \exp\left(\frac{-2z}{d_p} \right) dz \quad (8)$$

Substitution of eq 6 into eq 8 and integration yields:[25]

$$\frac{A(t) - A_0}{A_{eq} - A_0} = 1 - \frac{8}{\pi d_p [1 - \exp(-2\ell/d_p)]} \times \sum_{n=0}^{\infty} \frac{1}{2n+1} \left[\frac{\exp(-f^2 D_{eff} t)[f \exp(-2\ell/d_p) + (-1)^n 2/d_p]}{(2/d_p)^2 + f^2} \right] \quad (9)$$

where $A(t)$ is the infrared absorbance at time t, and A_{eq} is the absorbance value at equilibrium.

When $\ell/d_p > 10$, then eq 9 is equivalent to eq 6, where the concentration profile is essentially constant in the sampling region close to the polymer/crystal interface ($z = 0$) resulting in a spatially independent solution:

$$\frac{A(t) - A_0}{A_{eq} - A_0} = \frac{C - C_0}{C_{eq} - C_0} = 1 - \frac{4}{\pi} \times \sum_{n=0}^{\infty} \frac{(-1)^n}{2n+1} \exp(-D_{eff} f^2 t) \quad (10)$$

This is referred to as the thick film approximation.[26] In this study, $\ell/d_p \gg 10$, where $d_p \sim 1$ μm and $\ell \sim 180$ μm. Diffusion profiles (infrared absorbance as a function of time) can be regressed to eq 10 with the binary diffusion coefficient of water in Nafion (D_{eff}) being the only adjustable parameter in this model. Numerous diffusion experiments were conducted at each relative humidity. Immediately following each experiment, the Nafion membrane thickness was measured with a digital micrometer (Mitutoyo) with 1 μm accuracy (see Table 1). These thicknesses were used in the calculation of each diffusion coefficient to accurately account for the increase in thickness with increasing humidity. Each thickness measurement was the average of five readings at different positions on the membrane. The average standard deviation was 4% of the average thickness.

Results

Diffusion−Reaction. Figure 3a shows time-resolved infrared spectra for a low-humidity diffusion experiment: 22% RH water vapor diffusion into dry Nafion 117 (referred to as 0−22% RH). The inset in Figure 3a shows more clearly the infrared bands that are associated with the diffusion of water in the polymer (bands increasing with time) and the dissociation of sulfonic acid groups covalently attached to the polymer (bands decreasing with time) in the sampling region close to the polymer−crystal interface (evanescent wave). Water bands are represented by O−H stretching at 3374 cm^{-1}, H−O−H bending at 1630 cm^{-1},[27−29] and

Table 1. Water Diffusion Coefficients in Nafion

				this work		previous work[21]	
RH (%)	av RH (%)	λ^* (M_{H_2O}/M_{SO_3})	l (μm)	$D_w \times 10^7$ (cm^2/s)	this work SSE[c]	$D_w \times 10^7$ (cm^2/s)	SSE[c]
0−22	11	2.27	132 ± 2	4.44 ± 0.73[a]	0.108 ± 0.050	2.37 ± 0.84	0.66 ± 0.22
0−43	21	3.11	138 ± 3	4.39 ± 0.20[a]	0.073 ± 0.028	3.19 ± 0.32	0.44 ± 0.37
0−56	28	3.58	137 ± 3	7.95 ± 1.46[a]	0.074 ± 0.023	5.23 ± 0.87	0.33 ± 0.36
0−80	40	5.63	142 ± 2	4.35 ± 0.17[a]	0.051 ± 0.028	3.28 ± 0.37	0.024 ± 0.012
0−100	50		180 ± 12	7.50 ± 1.41[b]	0.108 ± 0.023	4.73 ± 0.54	0.47 ± 0.11
0−22	11					2.92 ± 0.59	0.89 ± 0.31
22−43	32					8.57 ± 2.68	0.066 ± 0.041
43−56	49					5.64 ± 0.91	0.12 ± 0.07
56−80	68					5.25 ± 1.25	0.19 ± 0.21
80−100	90					3.95 ± 2.10	0.51 ± 0.91

[a] Diffusion−reaction results. [b] Diffusion−relaxation results. [c] Sum of the squared error between model and data normalized by number of data points.

$(H-O-H)_nH^+$ bending at 1724−1684 cm^{-1}; the latter represents protonated water.[30] Anhydrous sulfonic acid (SO_3H) bands are represented by O−H stretching at 2758−2731[30] and 2204−2199 cm^{-1}.[31]

To examine water diffusion in Nafion, the water O−H stretching band was integrated from 3751 to 2983 cm^{-1} at each time point and the integrated absorbance plotted versus time. Figure 3b shows the integrated absorbance, normalized to the final value, versus time. The solid line in Figure 3b represents a regression to the Fickian diffusion model (eq 10), where the diffusion coefficient was the only adjustable fitting parameter. The poor regression suggests a form of non-Fickian or anomalous diffusion of water in Nafion for low-humidity vapor. Although upon visual inspection the data appears to look Fickian, the extended initial time lag seems to be the result of the observed non-Fickian behavior. It should be noted that the time lag in the data is an initial delay that is longer than that predicted by the Fickian model with the initial and boundary conditions specific to this ATR experiment (where the measurement takes place in the region near the polymer−crystal interface at the no flux boundary (eq 10)). This 0−22% RH experiment was repeated many times and the extended time lag was observed in all experiments and was not an artifact of any experimental error.

The time-resolved infrared spectra in Figure 3a provides evidence for the dissociation of anhydrous sulfonic acid during diffusion. Therefore, the extended time lag for low humidity experiments may be the result of this reaction between water and sulfonic acid in the polymer when the initial water molecules sorb into dry Nafion.

$$H_2O + SO_3H \leftrightarrow H_3O^+ + SO_3^- \qquad (11)$$

This reaction may prolong the time it takes for water to reach the polymer−crystal interface (where the absorbance of water is detected) resulting in this extended time lag. Specifically, the reaction converts water into protonated water. At low humidities, protonated water strongly interacts with immobile SO_3^- groups in the polymer. Therefore, at initial stages of sorption, the water content of the polymer is small, where a significant fraction of water will be initially consumed and converted into protonated water resulting in an observable time lag. For higher humidities, the fraction of water in the polymer is much higher and since the number of SO_3^- groups are fixed, a smaller fraction of water is consumed resulting in the apparent Fickian behavior observed in previous work.[21] Interestingly, the time-resolved FTIR−ATR spectra provides experimental evidence for all four species in the dissociation reaction (eq 11), where in addition to the water,

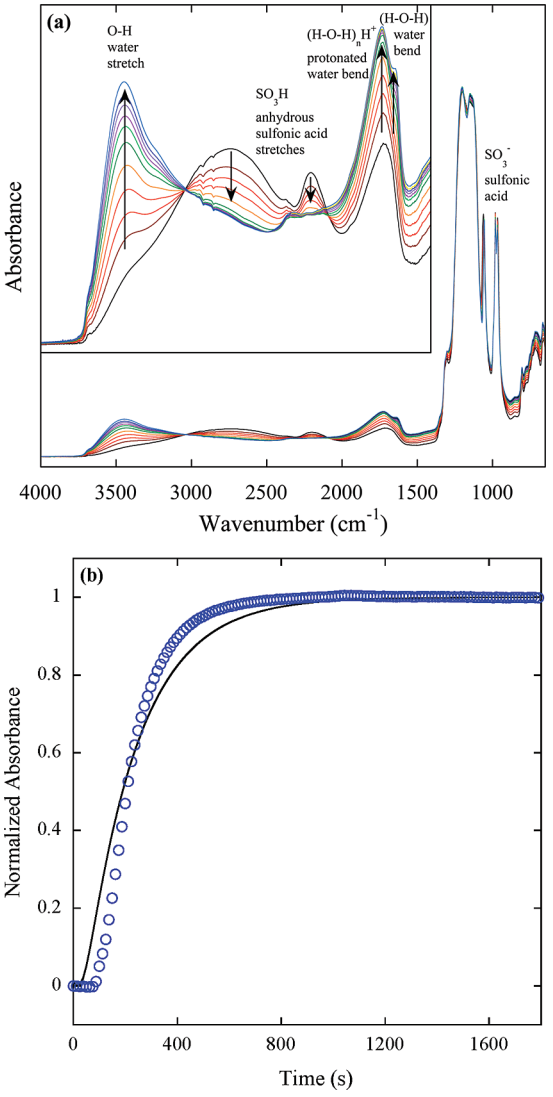

Figure 3. (a) Infrared spectra of water vapor (22% RH) diffusing into dry Nafion. Inset shows increase of the O−H stretching and $(H-O-H)_nH^+$ bending bands as a function of time as well as the decrease of SO_3H stretching bands with time. Arrows show direction of spectral change with increasing hydration. (b) Normalized, integrated absorbance of water O−H stretching (○). The line represents an optimized regression to the Fickian model (eq 10).

anhydrous sulfonic acid, and protonated water bands observed in Figure 3a, a band for the hydrolyzed sulfonated anion, SO_3^-, was observed at 1060 cm^{-1} (not shown in the inset of Figure 3a). In addition, as predicted from the

stoichiometric reaction, the rate of SO_3H decrease matches the rate of increase in $(H_2O)_nH^+$ and SO_3^- and is on the same time scale as the time lag in H_2O sorption. This experimental evidence of the reaction at low humidities further supports the theory that the reaction consumes water and causes the extended initial time lag at low humidities.

On the basis of these experimental observations, a mathematical model was developed that incorporates both diffusion and reaction.[22] For this system, a reaction can be written as

$$\underset{(W)}{H_2O} + \underset{(A)}{SO_3H} \xrightarrow{k_f} \underset{(H)}{H_3O^+} + \underset{(S)}{SO_3^-} \tag{12}$$

where W, A, H, and S are H_2O, SO_3H, H_3O^+, and SO_3^-, respectively, and k_f represents the forward reaction rate constant. An irreversible reaction was assumed because the equilibrium constant of an acid of similar strength, trifluoromethanesulfonic acid (triflic acid), in an equimolar water mixture is $\sim 10^{45}$, which was calculated from a Hammett acidity function value of -13.7.[32] In addition, the absorbances of anhydrous sulfonic acid in Figure 3a decrease to the baseline in approximately half the time it takes the water absorbance to reach equilibrium, suggesting the forward reaction is strongly favored. The one-dimensional continuity equations for these species are

$$\frac{\partial C_W}{\partial t} = D_W \frac{\partial^2 C_W}{\partial z^2} - r_W \tag{13}$$

$$\frac{\partial C_A}{\partial t} = -r_A \tag{14}$$

where water (W) is a mobile diffusing species and anhydrous sulfonic acid (A) is treated as an immobile species since it is covalently attached to the polymer. Also, in eqs 13 and 14, D_W is the diffusion coefficient of water in Nafion and r_W and r_A are the reaction rates for water and sulfonic acid, respectively. If the irreversible dissociation reaction can be treated as elementary then

$$-r_W = -r_A = kC_WC_A \tag{15}$$

This model can now be applied to the data to predict the time lag and accurately determine the diffusion coefficient of water in Nafion. In order to do this, the coupled species continuity equations (eqs 13 and 14) were solved numerically. The following equations represent dimensionless concentrations, time, and space and were used to convert eqs 13 and 14 into dimensionless form.

$$\theta_W = \frac{C_W}{C_W^f} \tag{16}$$

$$\theta_A = \frac{C_A}{C_A^o} \tag{17}$$

$$\tau = \frac{D_W t}{\ell^2} \tag{18}$$

$$\zeta = \frac{z}{\ell} \tag{19}$$

where C_W^f and C_A^0 are the equilibrium concentration of water in Nafion and the initial concentration of anhydrous sulfonic acid in dry Nafion (determined from the ion exchange capacity of Nafion), respectively. Recasting eqs 13 and 14 with the use of these dimensionless variables results in

$$\frac{\partial \theta_W}{\partial \tau} = \frac{\partial^2 \theta_w}{\partial \zeta^2} - \alpha \theta_w \theta_A \tag{20}$$

$$\frac{\partial \theta_A}{\partial \tau} = -\lambda^* \alpha \theta_W \theta_A \tag{21}$$

where

$$\alpha = \frac{C_A^o k_f \ell^2}{D_W} \tag{22}$$

$$\lambda^* = \frac{C_W^f}{C_A^o} \tag{23}$$

In eqs 22 and 23, α is the Damköhler number (ratio of the rate of reaction to diffusion) and λ^* is a measure of equilibrium water concentration in the polymer normalized to the initial concentration of sulfonic acid in the polymer. Because Nafion swells in water, the volume basis for initial and final concentrations are different, yielding units of mol (H_2O) L (dry Nafion)/mol (SO_3H) L (wet Nafion) for λ^*. The initial conditions recast into dimensionless form (at $\tau = 0$ for all ζ) become

$$\theta_W(0, \zeta) = 0 \tag{24}$$

$$\theta_A(0, \zeta) = 1 \tag{25}$$

The dimensionless boundary conditions for water at $\tau > 0$ are

$$\theta_W(\tau, 1) = 1 \tag{26}$$

$$\frac{\partial \theta_W(\tau, 0)}{\partial \zeta} = 0 \tag{27}$$

An explicit forward time, centered space (FTCS) algorithm was used to solve this system of equations, where the space domain was divided into 100 node points and each experimental time step was divided into 1000 node points.

A parametric study was first conducted on the numerical solution to probe the effect of α and λ^* on sorption kinetics. Figure 4a shows the effect of changing α for a fixed value of $\lambda^* = 2.27$. When $\alpha \ll 1$, the reaction kinetics are much slower than diffusion (reaction limiting), which results in Fickian behavior, which was expected since no reaction occurs on the time scale of diffusion. For $\alpha \sim 1$, the rate of reaction and diffusion are on similar time scales resulting in a type of anomalous behavior. For $\alpha \gg 1$, the reaction is much faster than diffusion (diffusion limiting), which interestingly results in an extended initial time lag followed by the appearance of Fickian-like sorption kinetics similar to what was observed experimentally in Figure 3b. Also, experimentally, the assumption of a high Damköhler number seems reasonable when accounting for the high dissociation constant of triflic acid. Therefore, the diffusion−reaction model with irreversible reaction, immobile sulfonic acid, and high Damköhler number (diffusion limiting) produces similar behavior with extended time lag as was observed experimentally. These results suggest that this could have an impact on fuel cell start up dynamics, where start up from dry to low humidities could result in a lag in performance on the order of minutes.

Figure 4b shows the effect of λ^* under the diffusion limiting case ($\alpha \gg 1$). Interestingly, the extended time lag is a function

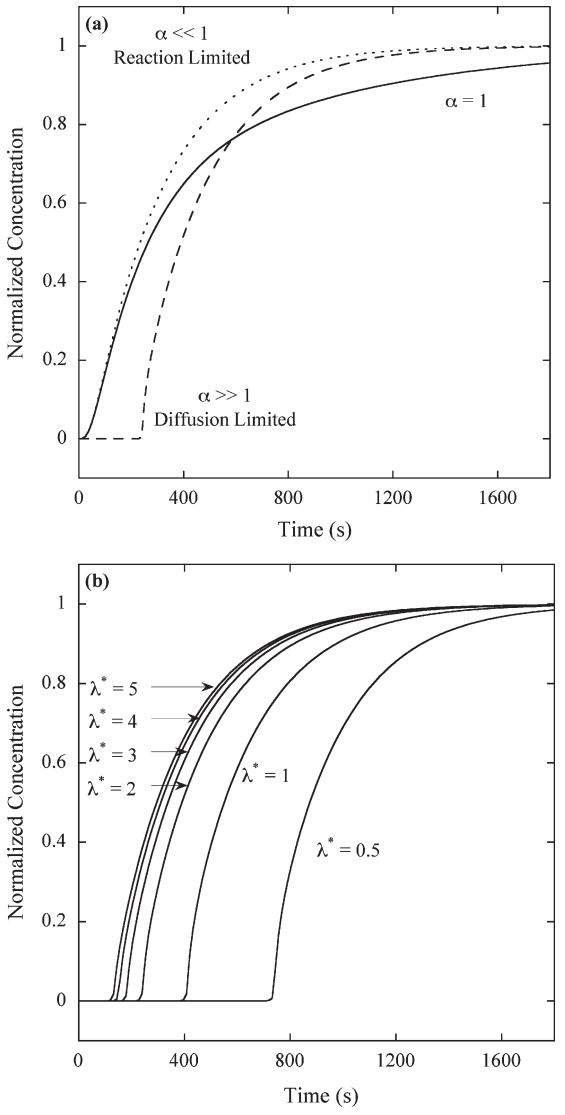

Figure 4. Parametric study of the diffusion−reaction model, where the parameter being varied is (a) the Damköhler Number, α, ($\lambda^* = 2.27$) and (b) final water content, λ^* ($\alpha \gg 1$).

of λ^*, where the time lag increases with decreasing λ^*. Also, as λ^* increases, the model approaches Fickian behavior under the diffusion limiting case. Physically, this seems reasonable since at lower water contents, a larger fraction of water molecules entering the polymer are consumed by a constant number of sulfonic acid sites. At higher water contents, a much smaller fraction of water is consumed, resulting in apparent Fickian behavior (no noticeable extended time lag). The results in Figure 4b were also observed experimentally, where the 0−22% RH experiment was non-Fickian with an extended time lag, but for other integral experiments (0−43, 0−56, 0−80% RH), apparent Fickian behavior was observed.

Equilibrium water sorption isotherms in Nafion have been measured with gravimetry by many investigators[33−43] with good agreement and are usually reported as a function of λ (mol (H_2O)/mol (SO_3H)). λ is calculated by normalizing the water gain by IEC (0.91 mmol (SO_3H)/g (dry Nafion)). However, diffusion and reaction rates are calculated on a concentration basis (λ^*), which is related to λ

$$C_W = \frac{\lambda \rho_{Nafion}}{(IEC/1000)} \tag{28}$$

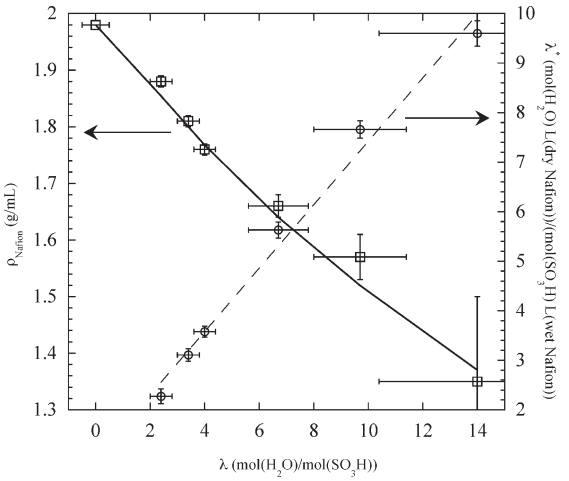

Figure 5. Dilation results showing Nafion density (□; left axis) and λ^* (○; right axis) as a function of gravimetric water content from literature (λ). The solid line is calculated density that assumes volume additivity between Nafion and water, while dotted line represents a trend line.

where ρ_{Nafion} is density (g (dry Nafion)/total volume). In other words, concentration is normalized by volume, which changes with humidity, while λ is normalized by the acid loading, which is constant. Volume was measured in this study (to determine ρ_{Nafion}) as a function of water vapor activity. Results are shown in Figure 5 as a function of the water content, λ. The solid line in Figure 5 is a calculated density using volume additivity (between water (1.0 mL/g) and Nafion (0.5 mL/g)) assuming no volume change upon mixing. The agreement is surprising because volume additivity between hydrated Nafion and methanol (with the assumption of no volume change upon mixing) did not match dilation data.[44] It should be noted that the Nafion density calculated at 100% RH has a large error, 70% of which comes from the error in the measurement of λ. This is because there is a steep upturn in the water sorption isotherm near activity of 1 (100% RH). The error in ρ_{Nafion} at lower activity is much smaller, as shown in Figure 5. λ^* for the diffusion−reaction model is calculated as water concentration, C_w^f, divided by sulfonic acid concentration, C^0_A = 1.8 mol/L. Figure 5 shows λ^* as a function of λ. While the difference between the λ^* and λ is not significant, it does vary by the factor (volume of wet Nafion)/(volume of dry Nafion). It is interesting to note that the change in dilation (Figure 5) and thickness (Table 1) are in good agreement.

With known values of λ^* (2.27), ℓ (0.0131 cm), α ($\gg$ 1), the data in Figure 3b was regressed to the numerical diffusion−reaction model, where D_W was the only adjustable fitting parameter. The results are shown in Figure 6. Unlike the poor regression to the Fickian model shown in Figure 3b, the diffusion−reaction model provides an adequate regression to the data with only one fitting parameter. The diffusion−reaction model was regressed to other integral diffusion experiments (0−43, 0−56, and 0−80% RH). The results of all these regressions are listed in Table 1. When comparing regressions from the diffusion−reaction model to regressions from the Fickian model (shown in Table 1), the errors between model and data all appear to be an order of magnitude lower for the diffusion−reaction model with a slight increase in regressed diffusion coefficients. Interestingly, although the error is lower for all of these experiments for the diffusion−reaction model, only the 0−22% RH visibly appears non-Fickian (**see** Figure 3b). In other words, the other integral diffusion experiments (0−43, 0−56, and

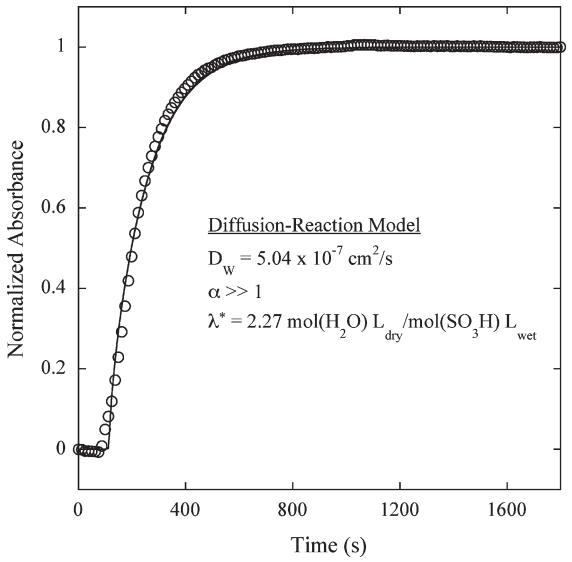

Figure 6. Regression of the diffusion−reaction model ($\lambda^* = 2.27$; $\alpha \gg 1$) to the normalized, integrated water O−H stretching absorbance, where the diffusion coefficient was the only fitting parameter.

0−80% RH) visually appear to regress to the Fickian model quite well.[21] It is also interesting to compare the diffusion−reaction model results to the differential experiments regressed to the Fickian model (also listed in Table 1). The errors between data and the Fickian model for smaller activity steps are comparable to the errors from the diffusion−reaction model. For example, the 0−56% RH integral experiments have an average RH of 28% and a diffusion coefficient of $(7.95 \pm 1.46) \times 10^{-7}$ cm^2/s when regressed to the diffusion−reaction model, while the 22−43% RH differential experiments have an average RH of 32% (similar to the 0−56% RH experiment) and a diffusion coefficient of $(8.57 \pm 2.68) \times 10^{-7}$ cm^2/s when regressed to the Fickian model. Therefore, even though the Fickian model provides a visibly good regression to integral diffusion experiments at 0−43, 0−56, and 0−80% RH, the diffusion−reaction model appears to provide more accurate diffusion coefficients when compared to the more accurate differential diffusion experiments (where smaller activity steps provide not only more accurate concentration-averaged Fickian diffusion coefficients but also initially hydrated conditions that reduce the effect of reaction).

Diffusion−Relaxation. Figure 7a shows time-resolved infrared spectra for an integral high-humidity diffusion experiment: 100% RH water vapor diffusion into dry Nafion 117 (referred to as 0−100% RH). At high wavenumber, the stretching and bending vibrations associated with water and anhydrous sulfonic acid are shown. Similar to Figure 3a, the bands associated with water and protonated water increase, while the bands associated with anhydrous sulfonic acid decrease with time. At lower wavenumber, the fingerprint region of the mid-infrared spectrum shows a number of stretching vibrations associated with functional groups in the backbone and side chain of the polymer: C−F_2 stretching (backbone) at 1250−1198 cm^{-1},[45−47] symmetric sulfonate anion, S−O_3^-, stretching (side chain) at 1060 cm^{-1},[45,48−51] and asymmetric and symmetric ether, C−O−C, stretching (side chain) at 982 and 967 cm^{-1}, respectively.[45,46,48,51] All of the absorbance bands associated with the polymer decrease with time as the water diffuses into the polymer. Figure 7b shows the normalized, integrated areas of the O−H stretching (water), backbone C−F_2 stretching, side-chain sulfonate anion (S−O_3^-) stretching, and side-chain ether (C−O−C) stretching

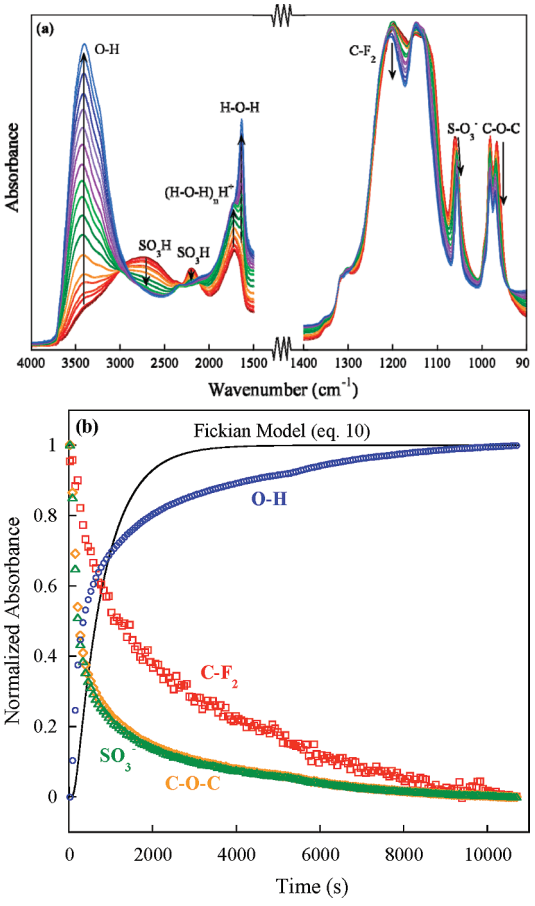

Figure 7. (a) Infrared spectra of water vapor (100% RH) diffusing into dry Nafion. The left and right sections of spectra are on different absorbance scales for clarity. Arrows show direction of spectral change with increasing hydration. (b) Normalized, integrated absorbance of water O−H stretching (○), polymer backbone C−F_2 stretching (□), sulfonate anion S−O_3^- symmetric stretching (△), and polymer side-chain C−O−C stretching (◇) versus time..

bands as a function of time. All of the integrated absorbance values shown in Figure 7b were initialized by their minimum value and normalized to their maximum value. The solid line in Figure 7b represents a regression of the water O−H stretching to the Fickian diffusion model (eq 10), where the diffusion coefficient was the only adjustable fitting parameter. The Fickian model does not regress well to this data, but appears to be a much different form of non-Fickian behavior than what was observed with the low-humidity differential experiment (Figure 3b). Other investigators have observed similar water sorption kinetics in Nafion for 0−100%RH from dynamic gravimetric experiments.[52,53] Others have also observed this type of non-Fickian behavior for the diffusion of organic vapors in glassy polymers.[23] These results are indicative of diffusion and polymer relaxation occurring at similar time scales. Nafion relaxation from the swelling stress induced by water has been measured by others and has been shown to be significant.[53] Also, since Nafion experiences a 37% increase in thickness from 0 to 100% RH,[21] this appears to be a reasonable explanation for the diffusion−relaxation phenomena that is observed. Additionally, the decrease in absorbance or concentration of polymer functional groups (Figure 7) also provides further experimental evidence of water-induced relaxation.

Interestingly, all of the polymer functional groups do not decrease at a similar rate. In Figure 7b, the side-chain sulfonate anion and ether groups appear to decrease at the

same rate, while the backbone CF_2 decreases at a slower rate. Also, the side-chain groups decrease at a similar rate to the increase in the water-stretching band. At first glance, the CF_2 dynamics appears erroneous and there does not seem to be a logical explanation for its difference compared to the other infrared bands. However, this data has been analyzed using a variety of methods and for numerous repeated experiments. These results are repeatable and are not a result of experimental error.

We postulate that these results are related to the morphology of Nafion. Although numerous research groups have developed differing morphological models for Nafion based on X-ray scattering data,[54−61] there is a consensus that Nafion possesses a cocontinuous phase-segregated morphology. The two phases are referred to as ion-rich (hydrophilic) and ion-poor (hydrophobic) regions, where electrostatic interactions between ion pairs results in interconnected ionic domains phase segregated from the surrounding ion poor regions. In relation to the experimental infrared data in Figure 7, the side chain sulfonate anion and ether groups reside in the hydrophilic ion rich domains, while the backbone CF_2 resides in the hydrophobic ion poor regions. Therefore, when water initially diffuses into the hydrophilic regions of the polymer, these domains are swollen, diluting the concentration of the hydrophilic regions of the polymer in the evanescent wave region close to the polymer/crystal interface. Experimentally, this results in a decrease in concentration or absorbance of the side chain sulfonate anion and ether groups and this decrease matches the rate of increase in water sorption. After the initial diffusion of water and swelling of hydrophilic regions, the swollen regions then impose stress on the surrounding hydrophobic matrix. This stress is dissipated via relaxation of the matrix and experimentally a dilution of CF_2 groups in the hydrophobic regions is observed with a decrease in absorbance in the evanescent wave. The morphology, therefore, explains the differences in the rate of swelling or relaxation and also suggest that the backbone CF_2 absorbance is a different measure of polymer relaxation and not a convolution of diffusion and relaxation as is observed with the absorbance of water and polymer groups in the hydrophilic ionic domain. This result is significant as it provides an independent measure of polymer relaxation in conjunction with diffusion−relaxation, which cannot be obtained with standard experimental techniques, such as dynamic gravimetry.

Therefore, with both a measure of diffusion−relaxation and relaxation within the same experiment, a mathematical model was developed that incorporates both diffusion and relaxation. For the relaxation portion of this model, a simple three-element viscoelastic model was used, shown schematically in Figure 8a. Here, a dashpot is in series with a dashpot and spring in parallel. The dashpot, which represents nonrecoverable viscous loss can be represented mathematically by Newton's law of viscosity:

$$\sigma = \eta \frac{\partial \varepsilon}{\partial t} \tag{29}$$

where σ, ε, and η are the stress, strain, and dynamic viscosity, respectively. The spring represents the purely elastic recoverable element that stores all energy used to perturb it from equilibrium and can be written mathematically as Hooke's law:

$$\sigma = E\varepsilon \tag{30}$$

where E is Young's modulus. The spring and dashpot in parallel represents a retarded elastic or viscoelastic response and this two-element portion is commonly known as the Kelvin (or Voigt) model. In relation to a creep experiment, in which a constant stress, σ_o, is applied and the strain (or elongation) is measured versus time, the Voigt model can be solved for strain:

$$\varepsilon = \frac{\sigma_o}{E}(1 - \exp(-\beta t)) \tag{31}$$

where β is the relaxation time constant (s^{-1}). The strain response with time for the two-element Voigt model is shown in Figure 8b. The strain of a simple dashpot is a linear function of time for a creep experiment:

$$\varepsilon = \frac{\sigma_o t}{\eta} \tag{32}$$

also shown in Figure 8b as the one-element setup. The three-element viscoelastic model is merely a sum of the

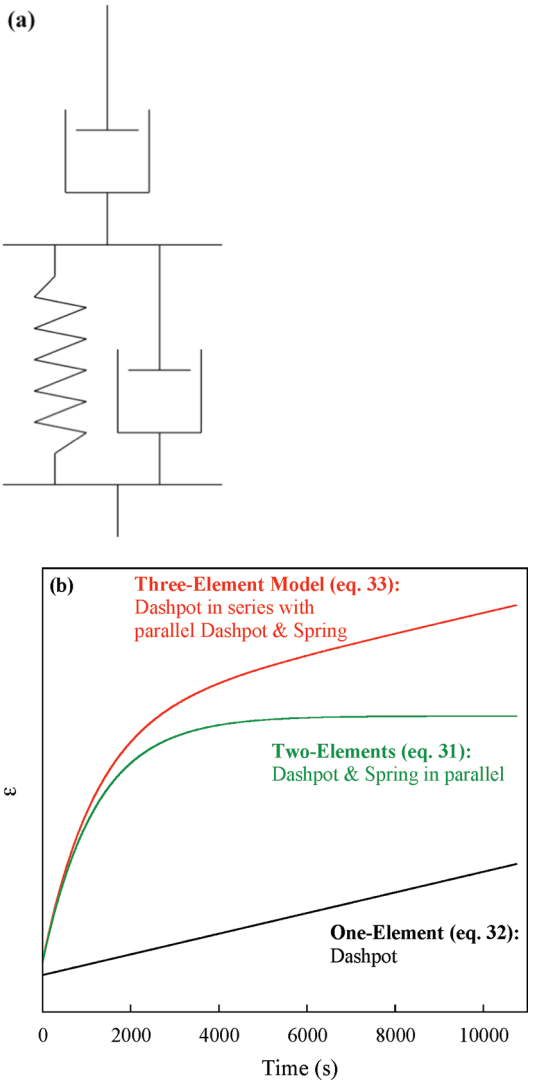

Figure 8. (a) Illustration of a three-element relaxation model consisting of a purely viscous dashpot in series with a dashpot and spring in parallel, where the spring is purely elastic. (b) Graphical representation of the strain response versus time for one-, two-, and three-element relaxation models based on a creep experiment, in which the stress is constant. The one-element model is a dashpot, the two-element model is a spring and dashpot in parallel, and the three-element model is that depicted in part a.

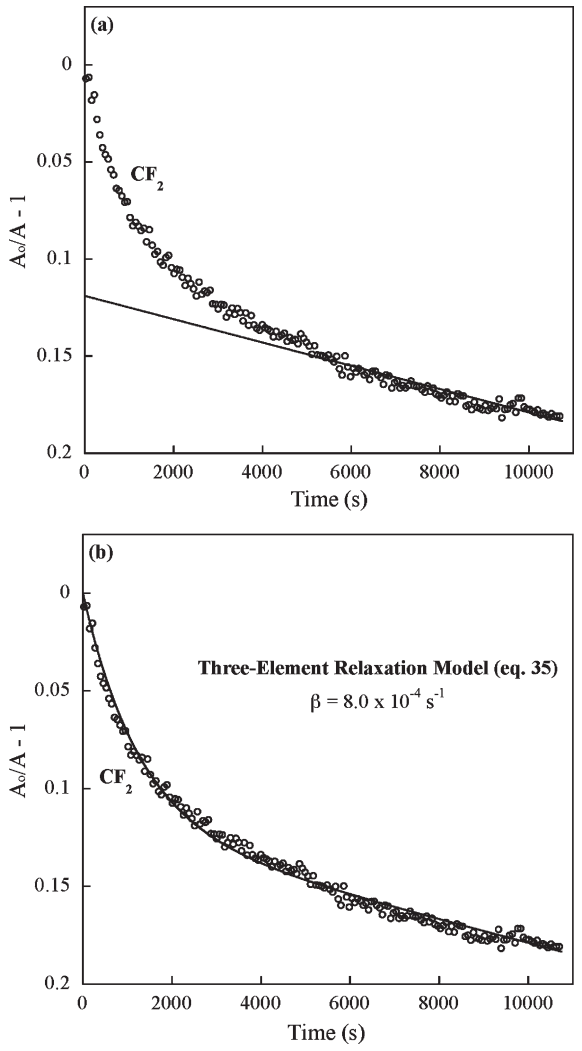

Figure 9. (a) Late-time, linear regression to polymer backbone C−F_2 stretching infrared absorbance in order to extract the weighting fractions of the relaxation model. (b) Regression of the relaxation model to the polymer backbone C−F_2 stretching infrared absorbance, where the relaxation time constant, β, was the only fitting parameter.

one-element dashpot and the two-element Voigt model:

$$\varepsilon = \frac{\sigma_o t}{\eta} + \frac{\sigma_o}{E}(1 - \exp(-\beta t)) \tag{33}$$

This three-element model is also shown in Figure 8b along with the one- and two-element components. In this model, we assume that stress, viscosity, and modulus are all constant. The polymer strain can be related to infrared absorbance data with the use of the Beer−Lambert law:

$$\varepsilon = \frac{\Delta V}{V_o} \approx \frac{1/C - 1/C_o}{1/C_o} \approx \frac{1/A - 1/A_o}{1/A_o} = \frac{A_o}{A} - 1 \tag{34}$$

where V_o, C_o, and A_o are the initial volume, concentration, and absorbance, respectively. Therefore, we propose that infrared absorbance of the polymer backbone groups are inversely proportional to strain or water-induced swelling. In other words, the inverse of the decrease in polymer absorbance or concentration due to relaxation is proportional to the strain in eq 34, and eq 33 can be rewritten in terms of experimental infrared absorbance of the CF_2 relaxation.

$$\frac{A_o}{A} - 1 = \frac{\sigma_o}{\eta} t + \frac{\sigma_o}{E}(1 - \exp(-\beta t)) \tag{35}$$

It is interesting to note that the strain or volumetric change ($A_o/A_f - 1$) from the infrared absorbance of the CF_2 relaxation in 0−100% RH experiments (0.20 ± 0.02) is on the same order of magnitude as the dilation experiments (data shown in Figure 5). For time-resolved data, a late-time solution to eq 35 only has a viscous contribution as the exponential term in the elastic portion goes to zero resulting in a linear equation, where the slope (σ_o/η) and intercept (σ_o/E) represent the mechanical constants of the dashpot and Voigt model, respectively. Figure 9a shows a linear regression of the late-time solution of eq 35 to the late-time CF_2 infrared absorbance, where $\sigma_o/\eta = 6 \times 10^{-6}$ Pa/Pa·s and $\sigma_o/E = 0.119$ Pa/Pa. According to Kawano et al.[62] Young's modulus of Nafion (E) is approximately 1 MPa. Therefore, using our regressed constants, the stress induced by Nafion swelling from dry to 100% RH is approximately 100 kPa. Then the average viscosity of the dashpot (the viscosity of the hydrophobic CF_2 polymer backbone) is approximately 20 GPa·s, which is reasonable for a solid polymer. With known constants from the late-time solution, the entire data set can be regressed to the full solution, eq 35, with only one adjustable parameter, the relaxation time constant, β. This regression is shown in Figure 9b with a regressed relaxation time constant of 8.0×10^{-4} s^{-1}. This value agrees well with literature, where a relaxation time on the order of 10^4 s was measured from creep experiments on humidified Nafion.[63] β is equal to the modulus divided by the viscosity of the Voigt dashpot (the viscosity of the hydrophilic, ionic domain). The viscosity of the hydrophilic domain of Nafion 117, 1 GPa·s, is an order of magnitude less than the hydrophobic domain.

The independent measurement of relaxation can be applied to the diffusion−relaxation data. A diffusion−relaxation model was developed and its solution can be described as a weighted sum of the diffusion solution (eq 10) and normalized relaxation (eq 35 normalized by final strain); similar in appearance to the Berens and Hopfenberg model.[23]

$$\frac{A(t) - A_o}{A_f - A_o} = F_A\left[1 - \frac{4}{\pi} \times \sum_{n=0}^{\infty} \frac{(-1)^n}{2n+1} \exp(-D_W f^2 t)\right] + F_B[w_2 t + w_1(1 - \exp(-\beta t))] \tag{36}$$

$$w_1 = \frac{\frac{\eta}{E}}{t_f + \frac{\eta}{E}} \tag{37}$$

$$w_2 = \frac{t_f}{t_f + \frac{\eta}{E}} \tag{38}$$

Equation 35 was normalized with respect to the strain at long times to incorporate into eq 36, where w_1 and w_2 are the dimensionless weighting fractions that result from this normalization. A comparison was performed between polymer absorbance strain data ($A_o/A - 1$) (eq 35) and normalized polymer absorbance data ($(A - A_o)/(A_f - A_o)$) (eq 36). The absorbance values differ by the factor A_f/A, which results in a maximum difference of less than 3%. The difference in mechanical constants obtained from regressing the two to the relaxation data was negligible. This exercise was carried out so as to incorporate the relaxation model (eq 35) into the diffusion−relaxation model (eq 36), where physically, water diffusion and polymer relaxation are coupled.

A more complex model was developed and regressed to this data. Using additional fitting parameters, the more complex model showed that a nonconstant stress (a function

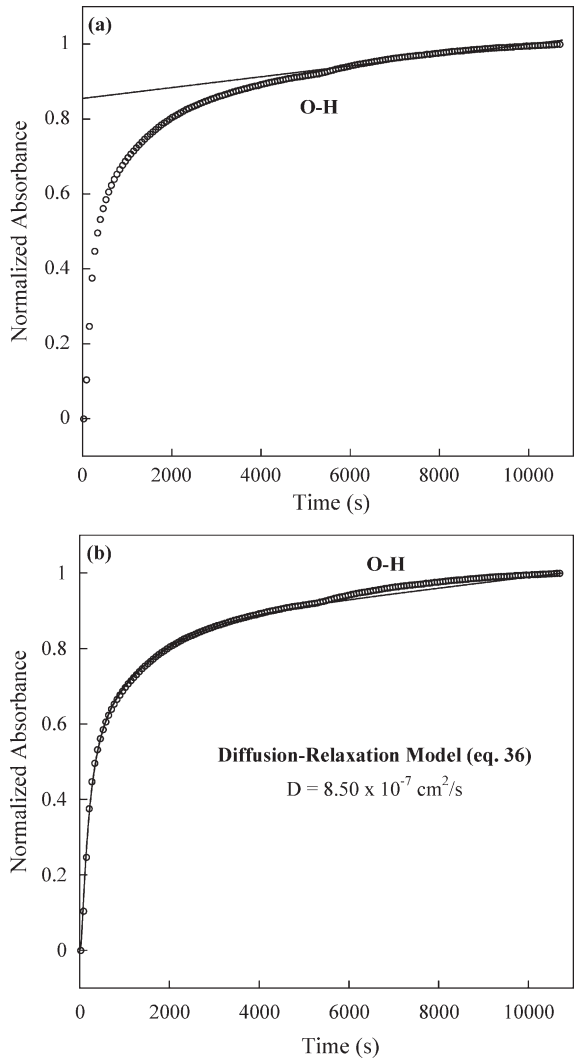

Figure 10. (a) Late-time, linear regression to water O−H stretching in order to extract the weighting fractions of the diffusion−relaxation model. (b) Regression of the diffusion−relaxation model to the normalized, integrated water O−H stretching absorbance, where the diffusion coefficient was the only fitting parameter.

of water concentration) changes rapidly at early time quickly reaching a constant value. In other words, the assumption of constant stress in this simple model was reasonable. The more complex model contained two additional springs so that polymer swelling could eventually come to equilibrium; i.e., the compressive stress of the polymer chains balance the swelling stress induced by water. The simple three-element model was recovered when this more complex model, with additional adjustable parameters, was regressed to the data, because the contribution of the additional springs were negligible on the time scale of the data.

Equation 36 then approximates water diffusion in Nafion as two contributions: one fraction caused by the concentration gradient of water and another from additional water sorption due to water-induced relaxation of the polymer or increased polymer free volume. Similar to the relaxation model, the late-time solution of the diffusion−relaxation model (eq 36) only represents the viscous loss portion of relaxation as the exponential terms in the diffusion and elastic portions approach zero at late times. Figure 10a shows a linear regression of the time-resolved water O−H stretching absorbance to the late-time solution of eq 36, where the slope ($F_B w_2$) and intercept ($F_A + F_B w_1$) are 0.155 and 0.855, respectively. Using normalized values of the mechanical constants from the late-time regression of the relaxation data in Figure 9a, the weighting fractions (F_A and F_B) for diffusion and relaxation can be determined and are both ~0.5. Now with known mechanical constants, the entire data set for water can be regressed to the full solution, eq 36, with only one adjustable parameter, the water diffusion coefficient, D_W. Figure 10b shows this with a diffusion coefficient of 8.50×10^{-7} cm^2/s.

Table 2. Diffusion−Relaxation Model Results (0-100% RH Experiment)

$\sigma_o/\eta \times 10^6$(Pa/Pa·s)	σ_o/E (Pa/Pa)	$\beta \times 10^4$ (s^{-1})	relaxation SSE[a]
5.0 ± 1.4	0.15 ± 0.04	8.27 ± 0.38	0.034 ± 0.031
F_A	F_B	D × 10^7 (cm^2/s)	SSE[a,b]
0.52 ± 0.05	0.48 ± 0.05	7.5 ± 1.4	0.11 ± 0.02

[a] Sum of the squared error between model and data normalized by number of data points. [b] On the basis of 867 data points opposed to 145 data points in other regressions.

For this experiment, a diffusion time ($\tau_D \sim l^2/D$) of 433 s can be calculated using a membrane thickness of 192 μm. This is slightly smaller (i.e., faster) than the relaxation time (β^{-1}) of 1210 s, but on the same order of magnitude. A diffusion Deborah number can be defined as polymer relaxation time divided by diffusion time.[64] When the diffusion Deborah number is large, indicative of glassy polymers, then polymer relaxation is much slower than diffusion, which follows Fick's law. When the diffusion Deborah number is on the order of 1 then both diffusion and relaxation contribute to the observed anomalous dynamics. Finally, Fickian diffusion should be recovered again when the diffusion Deborah number is much less than one. In this case, polymer relaxation is much faster than diffusion, as is the case for rubbery polymers. However for any experiment (such as FTIR−ATR) in which diffusion and relaxation are being measured simultaneously, the diffusion Deborah number cannot be less than one because stress relaxation is driven by diffusion. In other words, measured relaxation time cannot be faster than diffusion in such an experiment. For the integral experiment from 0 to 100% RH, a diffusion Deborah number of 2.8 was calculated (on the order of 1), which one would expect since the dynamics exhibit anomalous or non-Fickian behavior. Results from the diffusion−relaxation model analysis are listed in Tables 1 and 2, where all of the regressed values reported for the 0−100% RH experiment represent an average from repeated experiments.

The results from this diffusion−relaxation model for the integral experiment (large activity step) compare well with the analogous Fickian results for the differential experiment (small activity step). This comparison can be seen clearly in Table 1, where the 0−100% RH integral experiments have an average RH of 50% and a diffusion coefficient of (7.50 ± 1.41) × 10^{-7} cm^2/s when regressed to the diffusion−relaxation model, while the 43−56% RH differential experiments have an average RH of 49% (similar to the 0−100% RH experiment) and a diffusion coefficient of (5.64 ± 0.91) × 10^{-7} cm^2/s when regressed to the Fickian model. This is to be contrasted with a poor Fickian regression to the 0−100% RH integral experiments, which results in a diffusion coefficient of (4.73 ± 0.54) × 10^{-7} cm^2/s.

It is interesting to note the change in membrane thickness with humidity (water-induced strain): 132 ± 2 μm (22% RH), 142 ± 2 μm (80% RH), and 184 ± 11 μm (100% RH). The majority of thickness change occurs from 80 to 100% RH. This seems to corroborate with the diffusion−relaxation results, where ~50% of the contribution is due to

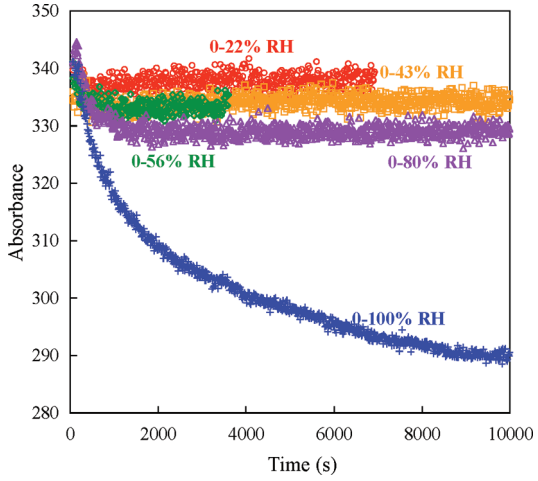

Figure 11. Time-resolved polymer backbone CF_2 stretching absorbance for 0−22% RH (○), 0−43% RH (□), 0−56% RH (◇), 0−80% RH (△), and 0−100% RH (+) water diffusion in Nafion.

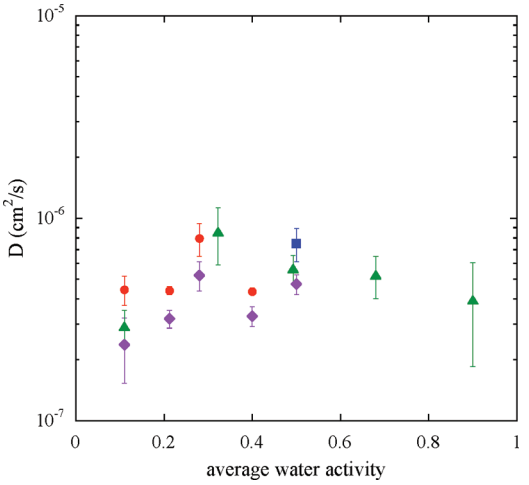

Figure 12. Water diffusion coefficients in Nafion from the diffusion−reaction model (●), the diffusion−relaxation model (■), the Fickian model for integral experiments (◆) and the Fickian model for differential experiments (▲) versus average water vapor activity.

water-induced relaxation. It is also interesting to note that because polymer relaxation is significant and slower in the 0−100% RH experiment, this results in experiments that are ~3 h opposed to ~30 min experiments for lower relative humidity experiments.

Although anomalous diffusion−relaxation phenomena was only observed for the 0−100% RH experiments, could it also be occurring at other relative humidities? In order to answer this question, the time-resolved absolute absorbance of the CF_2 stretching absorbance was plotted for the various experiments (shown in Figure 11). In comparison to the 0−100% RH experiment, the change in CF_2 absorbance (polymer relaxation) in other integral experiments (0−22, 0−43, 0−56, 0−80% RH) seem fairly insignificant. This corroborates with the apparent Fickian behavior observed in most of these experiments when examining the time-resolved water absorbance. Among these experiments, the 0−80% RH appears to show the most relaxation or swelling, which is still just a small fraction of the relaxation observed for the 0−100% RH. In addition, in the 0−80% RH experiment, there is no late time slope in relaxation data, suggesting that only viscoelastic (Voigt model) relaxation is occurring without any additional viscous loss. Therefore, the 0−80% RH backbone CF_2 stretching data was regressed to the two-element Voigt model, where the relaxation time constant was the only fitting parameter. The best fit resulted in a time constant, β, of 2.24×10^{-3} s^{-1} or a polymer relaxation time of 446 s, which was nearly identical to the diffusion time for this experiment, 452 s. The diffusion time was calculated from a diffusion coefficient of 4.44×10^{-7} cm^2/s and a thickness of 142 μm. This results in a diffusion Deborah number of ~1. Similar to the 0−100% RH experiments, a Deborah number of this order would suggest anomalous dynamics or that diffusion and relaxation are competing phenomena. However, this type of non-Fickian diffusion was not observed in the 0−80% RH experiments. In reality, since the relaxation time of the polymer is expected to decrease with increasing relative humidity, the polymer relaxation time in the 0−80% RH experiment is much longer than in the 0−100% RH experiment, so that the diffusion Deborah number for the 0−80% RH case is much larger than unity, and one observes only Fickian diffusion in the unrelaxed polymer matrix. This would suggest that at all humidities (measured in this study) less than 100% RH, any detectable polymer relaxation is actually elastic polymer swelling that has been induced by water diffusion. Only in the 0−100% RH experiment is there significant polymer relaxation that limits the kinetics and is therefore detectable in the FTIR−ATR experiment.

All of the results in Table 1 are shown in Figure 12, where diffusion coefficients, determined from Fickian regressions to all integral and differential experiments and diffusion−reaction and diffusion−relaxation regressions to integral experiments, are plotted as a function of average water vapor activity. The figure clearly shows that diffusion coefficients determined from the diffusion−reaction and diffusion−relaxation models appear more accurate with their match to Fickian diffusion coefficients determined from the differential experiments (with smaller activity steps; more accurate diffusion coefficients compared to integral experiments). However, the diffusion coefficients determined using the Fickian model on integral experiments does not grossly under predict water diffusivity and overall results still show that the water diffusivities in Nafion appear to be a weak function of water vapor activity.

Conclusions

Non-Fickian behavior was observed for both low humidity and high humidity experiments for water transport in Nafion. Time-resolved FTIR−ATR spectroscopy demonstrates that not only can water diffusion be measured, but also real-time molecular information for the acid dissociation reaction and polymer relaxation can be ascertained; the factors that cause the non-Fickian response. In this study, models that capture the diffusion−reaction and diffusion−relaxation phenomena with minimal fitting parameters were demonstrated. At low humidities (small concentration gradient), the diffusion−reaction model accurately accounts for the extended early time delay in water sorption kinetics, which was a result of the water-acid reaction and was a function of water concentration. At high humidity (high concentration gradient), the diffusion−relaxation model provides both a relaxation time constant and diffusion coefficient from separate data sets (polymer backbone relaxation and water sorption kinetics) from the same experiment (just different regions of the mid-IR spectra) with only one fitting parameter for each data set. This is a significant finding compared to previous work where a minimum of six fitting parameters were used to regress gravimetric data. This work demonstrates some of the capabilities of time-resolved FTIR−ATR spectroscopy for the investigation of polymer

dynamics. In particular, for the case of water−Nafion dynamics, new physical insights into the mechanisms regarding non-Fickian behavior were elucidated.

Acknowledgment. The authors acknowledge the financial support of the National Science Foundation (CARRER 0644593; IGERT 0221664) and the U.S. Army Research Office (W911NF-07-1-0149).

References and Notes

(1) Mathias, M. F.; Makharia, R.; Gasteiger, H. A.; Conley, J. J.; Fuller, T. J.; Gittleman, C. J.; Kocha, S. S.; Miller, D. P.; Mittelsteadt, C. K.; Xie, T.; Yan, S. G.; Yu, P. T. *Electrochem. Soc. Interface* **2005**, *14*, 24–35.
(2) Wee, J. H.; Lee, K. Y. *J. Power Sources* **2006**, *157*, 128–135.
(3) Yang, C.; Costamagna, P.; Srinivasan, S.; Benziger, J.; Bocarsly, A. B. *J. Power Sources* **2001**, *103*, 1–9.
(4) Grot, W. G. U.S. Patent 3,784,399, **1974**.
(5) Zawodzinski, T. A., Jr.; Neeman, M.; Sillerud, L. O.; Gottesfeld, S. *J. Phys. Chem.* **1991**, *95*, 6040–6044.
(6) Edmondson, C. A.; Fontanella, J. J. *Solid State Ionics* **2002**, *152−153*, 355–361.
(7) Hallinan, D. T., Jr.; Elabd, Y. A. *J. Phys. Chem. B* **2007**, *111*, 13221–13230.
(8) Morris, D. R.; Sun, X. *J. Appl. Polym. Sci.* **1993**, *50*, 1445–1452.
(9) Legras, M.; Hirata, Y.; Nguyen, Q. T.; Langevin, D.; Metayer, M. *Desalination* **2002**, *147*, 351–357.
(10) De Angelis, M. G.; Lodge, S.; Giacinti Baschetti, M.; Sarti, G. C.; Doghieri, F.; Sanguineti, A.; Fossati, P. *Desalination* **2006**, *193*, 398–404.
(11) Rivin, D.; Kendrick, C. E.; Gibson, P. W.; Schneider, N. S. *Polymer* **2001**, *42*, 623–635.
(12) Reineke, C. A.; Moll, D. J.; Reddy, D.; Wessling, R. A. Water Transport in Ionic Polymers. In *Water in Polymers*; American Chemical Society: Washington, DC, 1980; pp 69−84.
(13) Ye, X.; LeVan, D. *J. Membr. Sci.* **2003**, *221*, 147–161.
(14) Zelsmann, H. R.; Pineri, M.; Thomas, M.; Escoubes, M. *J. Appl. Polym. Sci.* **1990**, *41*, 1673–1684.
(15) Zhang, J.; Giotto, M. V.; Wen, W. Y.; Jones, A. A. *J. Membr. Sci.* **2006**, *269*, 118–125.
(16) Kreuer, K. D.; Paddison, S. J.; Spohr, E.; Schuster, M. *Chem. Rev.* **2004**, *104*, 4637–4678.
(17) Gong, X.; Bandis, A.; Tao, A.; Meresi, G.; Wang, Y.; Inglefield, P. T.; Jones, A. A.; Wen, W.-Y. *Polymer* **2001**, *42*, 6485–6492.
(18) Tsushima, S.; Teranishi, K.; Hirai, S. *Energy* **2005**, *30*, 235–245.
(19) Kim, M.-H.; Glinka, C. J.; Grot, S. A.; Grot, W. G. *Macromolecules* **2006**, *39*, 4775–4787.
(20) Pivovar, A. M.; Pivovar, B. S. *J. Phys. Chem. B* **2005**, *109*, 785–793.
(21) Hallinan, D. T., Jr.; Elabd, Y. A. *J. Phys. Chem. B* **2009**, *113*, 4257–4266.
(22) Catalano, J.; Giacinti Baschetti, M.; DeAngelis, M. G.; Sarti, G. C. *Desalination* **2009**, *240*, 341–346.
(23) Berens, A. R.; Hopfenberg, H. B. *Polymer* **1978**, *19*, 489–496.
(24) Piccinini, E.; Giacinti Baschetti, M.; Sarti, G. C. *J. Membr. Sci.* **2004**, *234*, 95–100.
(25) Elabd, Y. A.; Baschetti, M. G.; Barbari, T. A. *J. Polym. Sci., Part B: Polym. Phys.* **2003**, *41*, 2794–2807.
(26) Elabd, Y. A. Ph.D. Dissertation, Johns Hopkins University: **2000**.
(27) Buck, U.; Huisken, F. *Chem. Rev.* **2000**, *100*, 3863–3890.
(28) Rice, S. A.; Bergen, M. S.; Belch, A. C.; Nielson, G. *J. Phys. Chem.* **1983**, *87*, 4295–4308.
(29) Pereira, M. R.; Yarwood, J. *J. Chem. Soc., Faraday Trans.* **1996**, *92*, 2731–2735.
(30) Stoyanov, E. S.; Kim, K. C.; Reed, C. A. *J. Am. Chem. Soc.* **2006**, *128*, 1948–1958.
(31) Giguère, P. A.; Savoie, R. *J. Am. Chem. Soc.* **1963**, *85*, 287–289.
(32) Saito, S.; Saito, S.-i.; Ohwada, T.; Shudo, K. *Chem. Pharm. Bull.* **1991**, *39*, 2718–2720.
(33) Siu, A.; Schmeisser, J.; Holdcroft, S. *J. Phys. Chem. B* **2006**, *110*, 6072–6080.
(34) Choi, P.; Jalani, N. H.; Datta, R. *J. Electrochem. Soc.* **2005**, *152*, E84–E89.
(35) Pushpa, K. K.; Nandan, D.; Iyer, R. M. *J. Chem. Soc., Faraday Trans.* **1988**, *84*, 2047–2056.
(36) Morris, D. R.; Sun, X. *J. Appl. Polym. Sci.* **1993**, *50*, 1445–1452.
(37) Kreuer, K. D. *Solid State Ionics* **1997**, *97*, 1–15.
(38) Zawodzinski, T. A., Jr.; Neeman, M.; Sillerud, L. O.; Gottesfeld, S. *J. Phys. Chem.* **1991**, *95*, 6040–6044.
(39) Jalani, N. H.; Datta, R. *J. Membr. Sci.* **2005**, *264*, 167–175.
(40) Laporta, M.; Pegoraro, M.; Zanderighi, L. *Phys. Chem. Chem. Phys.* **1999**, *1*, 4619–4628.
(41) Jiang, R.; Kunz, H. R.; Fenton, J. M. *J. Power Sources* **2005**, *152*, A1329–A1340.
(42) Perrin, J.-C.; Lyonnard, S.; Guillermo, A.; Levitz, P. *J. Phys. Chem. B* **2006**, *110*, 5439–5444.
(43) Burnett, D. J.; Garcia, A. R.; Thielmann, F. *J. Power Sources* **2006**, *160*, 426–430.
(44) Hallinan, D. T., Jr.; Elabd, Y. A. Sorption and Diffusion Selectivity of Methanol/Water Mixtures in Nafion. In *Micro-Mini Fuel Cells—Fundamentals and Applications*; Kakac, S., Pramuanjaroenkij, A., Vasiliev, L., Eds.; Springer: Dordrecht, The Netherlands, 2008; pp 189−208.
(45) Givan, A.; Larsen, L. A.; Loewenschuss, A.; Nielsen, C. J. *J. Mol. Struct.* **1999**, *509*, 35–47.
(46) Gruger, A.; Regis, A.; Schmatko, T.; Colomban, P. *Vib. Spectr.* **2001**, *26*, 215–225.
(47) Colthup, N. B.; Daly, L. H.; Wiberley, S. E. *Introduction to Infrared and Raman Spectroscopy*, 3rd ed.; Academic Press: New York, 1990.
(48) Tan, S.; Bélanger, D. *J. Phys. Chem. B* **2005**, *109*, 23480–23490.
(49) Elabd, Y. A.; Napadensky, E. *Polymer* **2004**, *45*, 3037–3043.
(50) Pushpa, K. K.; Nandan, D.; Iyer, R. M. *J. Chem. Soc., Faraday Trans. 1* **1988**, *84*, 2047–2056.
(51) Ostrowska, J.; Narębska, A. *Colloid Polym. Sci.* **1983**, *261*, 93–98.
(52) Majsztrik, P. W.; Satterfield, M. B.; Bocarsly, A. B.; Benziger, J. B. *J. Membr. Sci.* **2007**, *301*, 93–106.
(53) Satterfield, M. B.; Benziger, J. B. *J.Phys. Chem. B* **2008**, *112*, 3693–3704.
(54) Gierke, T. D.; Munn, G. E.; Wilson, F. C. *J. Polym. Sci., Polym. Phys. Ed.* **1981**, *19*, 1687–1704.
(55) Schmidt-Rohr, K.; Chen, Q. *Nat. Mater.* **2008**, *7*, 75–83.
(56) Gebel, G.; Lambard, J. *Macromolecules* **1997**, *30*, 7914–7920.
(57) Rollet, A.-L.; Diat, O.; Gebel, G. *J. Phys. Chem. B* **2002**, *21*, 3033–3036.
(58) Rubatat, L.; Rollet, A.-L.; Gebel, G.; Diat, O. *Macromolecules* **2002**, *35*, 4050–4055.
(59) Haubold, H.-G.; Vad, T.; Jungbluth, H.; Hiller, P. *Electrochim. Acta* **2001**, *46*, 1559–1563.
(60) Kreuer, K. D. *J. Membr. Sci.* **2001**, *185*, 29–39.
(61) Kim, M.-H.; Glinka, C. J.; Grot, S. A.; Grot, W. G. *Macromolecules* **2006**, *39*, 4775–4787.
(62) Kawano, Y.; Wang, Y.; Palmer, R. A.; Aubuchon, S. R. *Polím.: Ciên. Tecnol.* **2002**, *12*, 96–101.
(63) Satterfield, M. B.; Majsztrik, P. W.; Ota, H.; Benziger, J. B.; Bocarsly, A. B. *J. Polym. Sci., Part B: Polym. Phys.* **2006**, *44*, 2327–2345.
(64) Vrentas, J. S.; Jarzebski, C. M.; Duda, J. L. *AIChE J.* **1975**, *21*, 894–901.
(65) Heitner-Wirguin, C. *J. Membr. Sci.* **1996**, *120*, 1–33.
(66) Grot., W. G. *Macromol. Symp.* **1994**, *82*, 161–172.